

Multifractal dimensions for critical random matrix ensembles

J. A. MÉNDEZ-BERMÚDEZ¹, A. ALCÁZAR-LÓPEZ¹ and IMRE VARGA^{2,3}

¹ *Instituto de Física, Benemérita Universidad Autónoma de Puebla, Apartado Postal J-48, Puebla 72570, Mexico*

² *Elméleti Fizika Tanszék, Fizikai Intézet, Budapesti Műszaki és Gazdaságtudományi Egyetem, H-1521 Budapest, Hungary*

³ *Fachbereich Physik und Wissenschaftliches Zentrum für Materialwissenschaften, Philipps Universität Marburg, D-35032 Marburg, Germany*

PACS 05.45.Df – Fractals

PACS 71.30.+h – Metal-insulator transitions and other electronic transitions

Abstract – Based on heuristic arguments we conjecture that an intimate relation exists between the eigenfunction multifractal dimensions D_q of the eigenstates of critical random matrix ensembles $D_{q'} \approx q D_q [q' + (q - q') D_q]^{-1}$, $1 \leq q \leq 2$. We verify this relation by extensive numerical calculations. We also demonstrate that the level compressibility χ describing level correlations can be related to D_q in a unified way as $D_q = (1 - \chi)[1 + (q - 1)\chi]^{-1}$, thus generalizing existing relations with relevance to the disorder driven Anderson-transition.

Introduction. – It is well-known that the spatial fluctuations of the eigenstates in a disordered system at the Anderson-transition show multifractal characteristics [1, 2] which has been demonstrated recently in a series of experiments [3]. Therefore the modeling and analysis of multifractal states has become of central importance producing many interesting results. For this purpose random matrix models have been invoked and studied recently [4–6].

Since the exact, analytical prediction of the multifractal dimensions of the states for the experimentally relevant Anderson-transition in $d = 3$ or the integer quantum-Hall transition in $d = 2$ seems to be out of reach, it is desirable to search for heuristic relations in order to understand the complexity of the states at criticality. In the present paper we propose such heuristic relations that are numerically verified using various ensembles of random matrices.

The spatial fluctuations of the eigenstates can be described by a set of multifractal dimensions D_q defined by the scaling of the inverse mean eigenfunction participation numbers with the system size N :

$$\left\langle \sum_{i=1}^N |\Psi_i|^{2q} \right\rangle \sim N^{-(q-1)D_q}, \quad (1)$$

where $\langle \dots \rangle$ is the average over some eigenvalue window and over random realizations of the matrix. For strongly localized eigenstates these quantities do not scale with system size, i.e. $D_q \rightarrow 0$ for all q , while extended states

always feel the entire system, i.e. $D_q \rightarrow d$ for all q . Multifractal states, on the other hand, should be described by the series of the D_q , which are a nonlinear function of the parameter q .

Spectral fluctuations can be characterized in many ways. A usual, often employed quantity is the level compressibility χ , which is extracted from the limiting behavior of the spectral number variance as $\Sigma^{(2)}(E) = \langle n(E)^2 \rangle - \langle n(E) \rangle^2 \sim \chi E$, where $n(E)$ is the number of eigenstates in an interval of length E . The spectral fluctuations in a metallic system with extended states yield a vanishing compressibility, $\chi \rightarrow 0$, while in a strongly disordered insulating system the levels are uncorrelated, so they are easily compressible, $\chi = 1$. However, for the multifractal states an intermediate statistics exists, $0 < \chi < 1$, furthermore the spectral and eigenstate statistics are supposed to be coupled, which has been pointed out first in Ref. [7].

One of the most important generalized dimensions often used in this context is the information dimension D_1 . It is defined through the scaling of the mean eigenfunction entropy with the logarithm of the system size:

$$\left\langle - \sum_{i=1}^N |\Psi_i|^2 \ln |\Psi_i|^2 \right\rangle \sim D_1 \ln N. \quad (2)$$

A further, well-known and widely used dimension is called the correlation dimension D_2 , which is extracted from the inverse participation number from Eq. (1) using $q = 2$.

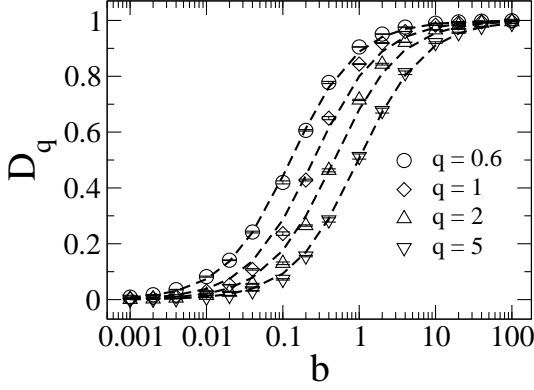


Fig. 1: D_q as a function of b for the PBRM model at criticality with $\beta = 1$. The dashed lines are fits of the numerical data with Eq. (8).

In a recent work [4] Bogomolny and Giraud have shown that in a d -dimensional critical system the information dimension D_1 and the level compressibility χ are simply related as

$$\chi + D_1/d = 1, \quad (3)$$

furthermore the generalized dimensions D_q can be expressed as

$$\frac{D_q}{d} = \begin{cases} \frac{\Gamma(q-1/2)}{\sqrt{\pi}\Gamma(q)}(1-\chi), & 1-\chi \ll 1 \\ 1-q\chi, & \chi \ll 1 \end{cases}. \quad (4)$$

These expressions have been shown to be valid for various critical random matrix ensembles in Ref. [4].

As for the critical, three-dimensional Anderson transition and the two-dimensional quantum-Hall transition it has been shown earlier that another relation holds between the level compressibility χ and the correlation dimension D_2 [7]:

$$2\chi + D_2/d = 1. \quad (5)$$

This relation should obviously hold approximately only since $0 \leq D_2/d \leq 1$ but $0 \leq \chi \leq 1$, leaving the range of validity for the limit of weak-multifractality.

In the present work we show a series of relations between various generalized dimensions, D_q and $D_{q'}$, and the level compressibility χ allowing for a generalization that for particular cases yields Eq. (3) exactly and Eq. (5) in the appropriate limit. In order to prove that, numerical simulations of various critical random matrix ensembles will be used. Further implications and more details will be presented elsewhere [8].

Model and heuristic relations. — In Ref. [4] Eqs. (3) and (4) were shown to be correct numerically for the Power-Law Banded Random Matrix (PBRM) model [2,9,10] at criticality. Below we will make use of this model to derive our main results.

The PBRM model describes one-dimensional (1d) samples of length N with random long-range hoppings. This

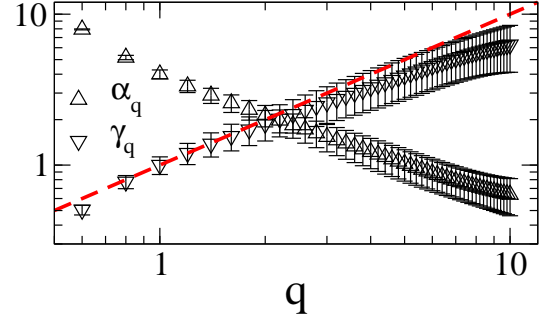


Fig. 2: α_q and $\gamma_q = \alpha_1/\alpha_q$ as a function of q for the PBRM model at criticality with $\beta = 1$. The red dashed line equal to q is plotted to guide the eye. The error bars are the rms error of the fittings.

model is represented by $N \times N$ real symmetric ($\beta = 1$) or complex hermitian ($\beta = 2$) matrices whose elements are statistically independent random variables drawn from a normal distribution with zero mean and a variance given by $\langle |H_{mn}|^2 \rangle = \beta^{-1}$ and

$$\langle |H_{mn}|^2 \rangle = \frac{1}{2} \frac{1}{1 + [\sin(\pi|m-n|/N)/(\pi b/N)]^{2\mu}}, \quad (6)$$

where b and μ are parameters. In Eq. (6) the PBRM model is in its periodic version; i.e. the 1d sample is in a ring geometry. Theoretical considerations [2,9–11] and detailed numerical investigations [2,12,13] have verified that the PBRM model undergoes a transition at $\mu = 1$ from localized states for $\mu > 1$ to delocalized states for $\mu < 1$. This transition shows all the key features of the disorder driven Anderson metal-insulator transition [2], including multifractality of eigenfunctions and non-trivial spectral statistics. Thus the PBRM model possesses a line of critical points $b \in (0, \infty)$ in the case of $\mu = 1$. In the following we will focus on the PBRM model at criticality, $\mu = 1$. By tuning the parameter b the states cross over from the nature of weak-multifractality ($b \gg 1$) which corresponds to extended-like or metallic-like states to strong-multifractality ($b \ll 1$) showing rather localized, i.e. insulator-like states. Meanwhile at the true, Anderson transition in $d = 3$ or at the integer quantum-Hall transition in $d = 2$, the states belong to the weakly multifractal regime, the PBRM model allows for an investigation without such a limitation. The evolution of the generalized dimensions as a function of the parameter b therefore represent this behavior, i.e. $D_q \rightarrow 1$ for $b \gg 1$ and in the other limit of $b \ll 1$ the multifractal dimensions vanish as $D_q \sim b$ [2,10].

Previously, for the PBRM model at criticality with $\beta = 1$, we have observed that both, D_1 and D_2 can be approximated simply as [14] $D_1 \approx [1 + (\alpha_1 b)^{-1}]^{-1}$ and $D_2 \approx [1 + (\alpha_2 b)^{-1}]^{-1}$ where $\alpha_{1,2}$ are fitting constants. This continuous function is a trivial interpolation between the limiting cases of low- b and large- b taking the half of

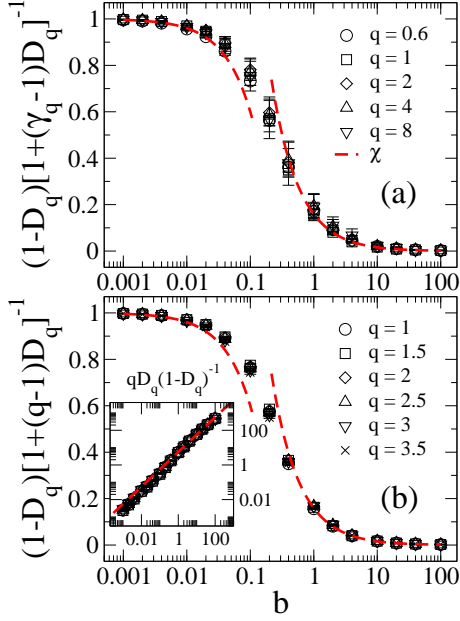


Fig. 3: (a) $(1 - D_q)[1 + (\gamma_q - 1)D_q]^{-1}$ and (b) $(1 - D_q)[1 + (q - 1)D_q]^{-1}$ [see Eqs. (11) and (12)] as a function of b for the PBRM model. The red dashed lines are the analytical prediction for χ given in Eq. (10). Inset in (b): $qD_q(1 - D_q)^{-1}$ as a function of b , see Eq. (16). The red dashed line equal to $\alpha_1 b$ is plotted to guide the eye.

the harmonic mean of the two as

$$\frac{1}{D_q} = 1 + \frac{1}{\alpha_q b}, \quad (7)$$

valid for $q = 1$ and 2 . Here we generalize and propose the following heuristic expression for a wider range of the parameter q

$$D_q \approx [1 + (\alpha_q b)^{-1}]^{-1}, \quad (8)$$

as a global fit for the multifractal dimensions D_q of the PBRM model in both symmetries, $\beta = 1$ and $\beta = 2$. In Fig. 1 we show fits of Eq. (8) to numerically obtained D_q as a function of b for some values of q and in Fig. 2 we plot the values of α_q extracted from the fittings.¹ We observe that Eq. (8) fits reasonably well the numerical D_q for $q > 1/2$. It is important to stress that Eq. (8) reproduces well the b -dependencies predicted analytically [2] for the limits $b \ll 1$ and $b \gg 1$. We noticed that by the use of Eq. (8), Eq. (3) leads to

$$\chi \approx (1 + \alpha_1 b)^{-1}, \quad (9)$$

which also reproduces well the b -dependencies predicted

¹ The multifractal dimensions D_q were extracted from the linear fit of the logarithm of the inverse mean eigenfunction participation numbers versus the logarithm of N , see Eq. (1). D_1 was extracted from the linear fit of the mean eigenfunction entropy versus the logarithm of N , see Eq. (2). We used $N = 2^n$, $8 \leq n \leq 13$. The average was performed over 2^{n-3} eigenvectors with eigenvalues around the band center with 2^{16-n} realizations of the random matrices.

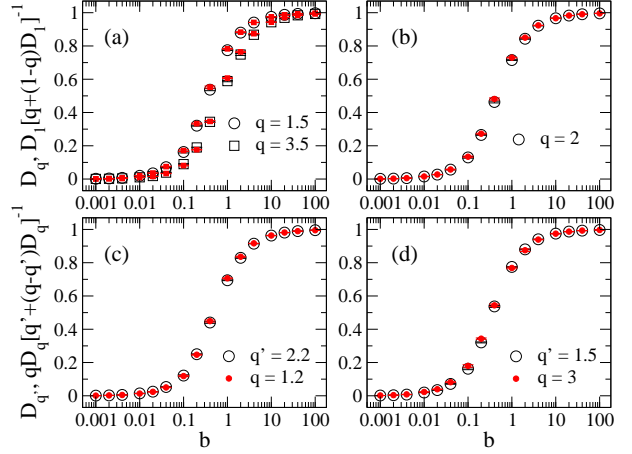


Fig. 4: (a-b) D_q (open symbols) and $D_1[q + (1 - q)D_1]^{-1}$ (full red symbols) [see Eq. (13)] and (c-d) $D_{q'}$ (open symbols) and $qD_q[q' + (q - q')D_q]^{-1}$ (full red symbols) [see Eq. (14)] as a function of b for the PBRM model.

analytically [2, 4] in the small- and large- b limits:

$$\chi = \begin{cases} 1 - 4b & b \ll 1 \\ (2\pi b)^{-1} & b \gg 1 \end{cases}. \quad (10)$$

Then, by equating b in Eqs. (8) and (9) we get

$$\chi \approx (1 - D_q)[1 + (\gamma_q - 1)D_q]^{-1}, \quad (11)$$

with $\gamma_q = \alpha_1/\alpha_q$. We observed that $\gamma_q \approx q$ in the range $0.8 < q < 2.5$, see Fig. 2, so in this range of q values we can write simplified relations between χ and D_q :

$$\chi \approx \frac{1 - D_q}{1 + (q - 1)D_q} \quad \text{and} \quad D_q \approx \frac{1 - \chi}{1 + (q - 1)\chi}. \quad (12)$$

The expression for D_q in Eq. (12) reproduces Eq. (4) exactly for $q = 1$ and $q = 2$ and approximately for $1 < q < 2.5$. Moreover, Eq. (12) combined with Eq. (3) allows us to express any D_q in terms of D_1 :

$$D_q \approx D_1 [q + (1 - q)D_1]^{-1}. \quad (13)$$

We also noticed that by equating χ for different D_q 's form Eq. (12) we could get recursive relations for them:

$$\frac{q'D_{q'}}{1 - D_{q'}} = \frac{qD_q}{1 - D_q} \quad \text{and} \quad D_{q'} = \frac{qD_q}{q' + (q - q')D_q}, \quad (14)$$

which lead to $D_{q+1} = qD_q(1 + q - D_q)^{-1}$, when $q' = q + 1$. These expressions also provide a relation between the correlation dimension and the information dimension or between the correlation dimension and the compressibility of the spectrum:

$$D_2 = D_1(2 - D_1)^{-1} = (1 - \chi)(1 + \chi)^{-1}. \quad (15)$$

It is relevant to add that in the weak multifractal regime, i.e. when $\chi \rightarrow 1$, Eq. (15) reproduces the relation given in Eq. (5) with $d = 1$, reported in [7].

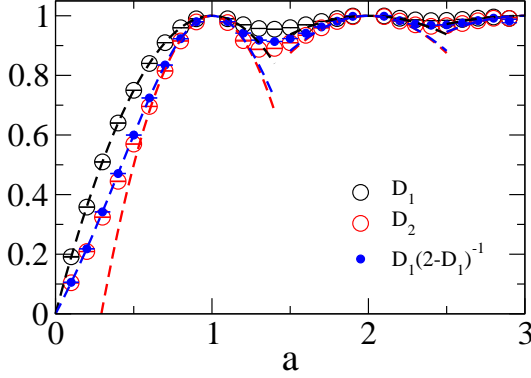


Fig. 5: D_1 , D_2 , and $D_1(2 - D_1)^{-1}$ as a function of a for the RSE (black open, red open, and blue full circles). Black and red dashed lines are the theoretical predictions for D_1 and D_2 , respectively, given in Eqs. (20) and (21). The blue dashed line is the prediction for D_2 given by Eq. (22).

Numerical results for the PBRM model. — Here we verify the expressions (11-15) for the PBRM model at criticality. Below we concentrate on the case $\beta = 1$ but we have already validated our results for $\beta = 2$.

In Fig. 3 we plot $(1 - D_q)[1 + (\gamma_q - 1)D_q]^{-1}$ and $(1 - D_q)[1 + (q - 1)D_q]^{-1}$ as a function of b for several values of q and observe good correspondence with the analytical prediction for χ ; that is, we verify the validity of Eqs. (11) and (12), respectively. In the inset of Fig. 3(b) we plot $qD_q(1 - D_q)^{-1}$ as a function of b , see Eq. (14), which for the PBRM model acquires the simple form

$$qD_q(1 - D_q)^{-1} \approx q\alpha_q b \approx \alpha_1 b. \quad (16)$$

Then, in Fig. 4 we compare D_q and $D_{q'}$ with $D_1[q + (1 - q)D_1]^{-1}$ and $qD_q[q' + (q - q')D_q]^{-1}$, respectively, for several values of q ; that is, we verify the validity of Eqs. (13) and (14). Eq. (15) is also validated in Fig. 4(b).

Additionally, in [15] the duality relation

$$D_2(B) + D_2(B^{-1}) = 1, \quad B \equiv 2^{1/4}\pi b, \quad (17)$$

was shown to be valid (with maximum deviations of 1%) for the PBRM model at criticality. We also want to comment that by the use of Eq. (8) we could write $D_2(B) \approx [1 + (\delta B)^{-1}]^{-1}$, with $\delta \equiv \alpha_2/(2^{1/4}\pi)$, so relation (17) gets the form

$$D_2(B) + D_2(B^{-1}) \approx 1 - \frac{B(\delta - 1)^2}{B + \delta(B^2 + \delta B + 1)}. \quad (18)$$

We notice that the quantity $D_2(B) + D_2(B^{-1})$ is very sensitive to the value of α_2 . So, the error in α_2 is magnified in the r.h.s. of Eq. (18). The maximal deviation from 1 (of 7.3% and 2% for $\beta = 1$ and $\beta = 2$, respectively) occurs at $B = 1$ where the r.h.s. of Eq. (18) acquires the form $1 - [(\delta - 1)/(\delta + 1)]^2$.

Other critical ensembles. — Remember that relations (12-15) were obtained from the combination of

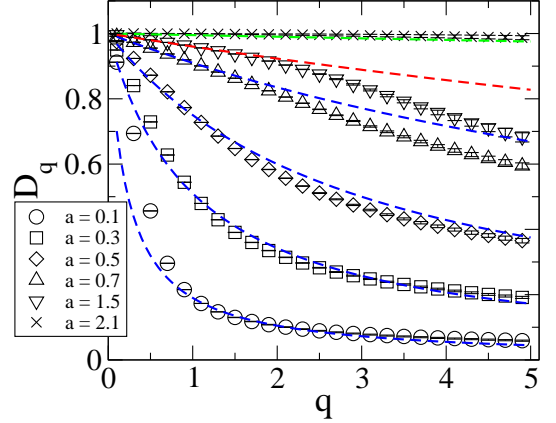


Fig. 6: D_q as a function of q for the RSE (black open symbols) for several values of a . Blue dashed lines are Eq. (23). The green dashed line is Eq. (24) with $k = 2$. The red dashed line is Eq. (13) with $D_1(a = 1.5) = 0.96$.

Eqs. (8) and (9). That is, relations (12-15) are expected to work in particular for the PBRM model at criticality. However, Eqs. (12) reproduce Eqs. (3) and (4), which were shown to be valid for the PBRM model but also for other critical ensembles [4]. Then the question is to which extent relations (12-15) are valid for critical ensembles different to the PBRM model. So, in the following we verify the validity of Eqs. (12-15) for other critical ensembles.²

The Ruijsenaars-Schneider Ensemble (RSE). The RSE proposed in [16] is defined as matrices of the form

$$H_{mn} = \exp(i\Phi_m) \frac{1 - \exp(2\pi i a)}{N[1 - \exp(2\pi i(m - n + a)/N)]}, \quad (19)$$

where $1 \leq m \leq n$, Φ_m are independent random phases distributed between 0 and 2π , and a is a free parameter independent on N . When $0 < a < 1$, the compressibility and the multifractal dimensions take the form [4]

$$\chi \sim (a - 1)^2 \quad \text{and} \quad D_q = 1 - q(a - 1)^2; \quad (20)$$

while in the vicinity of an integer $k \geq 2$, when $|a - k| \ll 1$,

$$\chi \sim (a - k)^2/k^2 \quad \text{and} \quad D_q = 1 - q(a - k)^2/k^2. \quad (21)$$

As shown in [4], Eqs. (20) and (21) satisfy relation (3). Moreover, by direct substitution of Eqs. (20) [or Eqs. (21)] we verified that Eqs. (12-15) are also satisfied at leading order in $(a - 1)^2$ [$(a - k)^2$].

In Fig. 5 we plot D_1 and D_2 as a function of a for the RSE. Black and red dashed lines are the theoretical predictions for D_1 and D_2 , respectively, given in Eqs. (20) and (21). As it was earlier shown in Ref. [4], the analytical form of D_q given in Eqs. (20) and (21) reproduces very well

² The multifractal dimensions D_1 and D_q for those ensembles were extracted numerically by the use of the same matrix sizes and ensemble realizations as for the PBRM model, if not indicated otherwise.

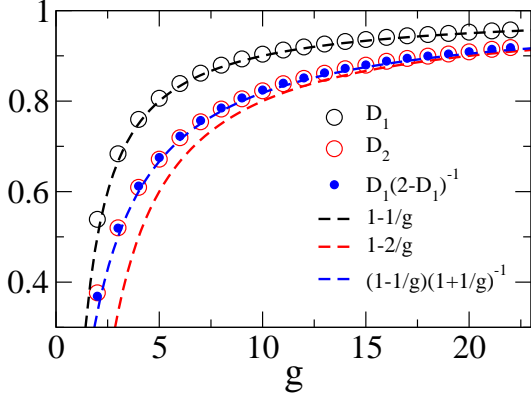


Fig. 7: D_1 , D_2 , and $D_1(2 - D_1)^{-1}$ as a function of g for the IQM model (black open, red open, and blue full circles). Black and red dashed lines are the theoretical predictions for D_1 and D_2 , respectively, given in Eqs. (25). The blue dashed line is the prediction for D_2 given by Eq. (26).

the numerically obtained D_1 . However, we notice that Eq. (20) does not describe well the numerical D_2 , mainly when $a \rightarrow 0$. Now, note that by plotting the numerically obtained $D_1/(2 - D_1)$ we get good agreement with the numerical data for D_2 , that is Eq. (15) works well for this model. Then, if we take $D_1 \approx 1 - (a - 1)^2$ and $D_1 \approx 1 - (a - k)^2/k^2$ as theoretical predictions for D_1 and plug them into Eq. (15) we get

$$D_2 \approx \frac{1 - (a - 1)^2}{1 + (a - 1)^2} \quad \text{and} \quad D_2 \approx \frac{k^2 - (a - k)^2}{k^2 + (a - k)^2}, \quad (22)$$

for $0 < a < 1$ and $|a - k| \ll 1$ with $k \geq 2$, respectively; which in fact work much better than $D_2 \approx 1 - 2(a - 1)^2$ and $D_2 \approx 1 - 2(a - k)^2/k^2$, correspondingly; see Fig. 5.

To get expressions for D_q we substituted $\chi \sim (a - 1)^2$ and $\chi \sim (a - k)^2/k^2$ [or $D_1 \approx 1 - (a - 1)^2$ and $D_1 \approx 1 - (a - k)^2/k^2$] into Eq. (12) [or Eq. (13)], to get

$$D_q \approx [1 - (a - 1)^2] [1 + (q - 1)(a - 1)^2]^{-1} \quad (23)$$

and

$$D_q \approx [k^2 - (a - k)^2] [k^2 + (q - 1)(a - k)^2]^{-1}. \quad (24)$$

In Fig. 6 we plot D_q as a function of q for the RSE for several values of a . We also plot Eqs. (23) and (24) and observe rather good correspondence with the numerical data mainly in the range $1 < q < 2$. Notice that neither Eq. (23) nor Eq. (24) can be used for $a = 1.5$. For that case we substituted the numerically obtained value of D_1 into Eq. (13) and again observe good correspondence for $0 < q < 2$, see the red dashed line in Fig. 6.

Intermediate quantum maps. A variant of the RSE was studied in [17] with the name of intermediate quantum maps (IQM) model. In this model the parameter a of the RSE equals cN/g with $cN = \pm 1 \bmod g$, being g the parameter of the IQM model. For the IQM model the

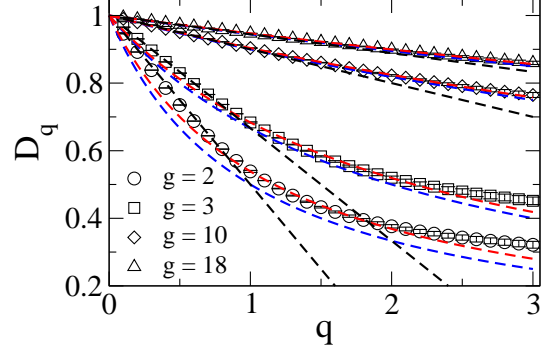


Fig. 8: D_q as a function of q for the IQM model (black open symbols) for $g = 2, 3, 10$, and 18 . Blue dashed lines are Eq. (27). Red dashed lines are Eq. (13) where the numerical values $D_1 = 0.538, 0.683, 0.904$, and 0.947 have been used for $g = 2, 3, 10$, and 18 , respectively. Black dashed lines are D_q from Eqs. (25).

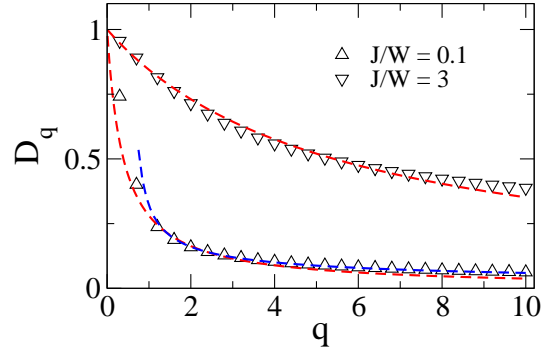


Fig. 9: D_q as a function of q for the CUE (taken from [18]). The blue dashed line is D_q from Eq. (29) for $J/W = 0.1$. Red dashed lines are the prediction for D_q given by Eq. (13) using $D_1 = 0.2805$ and 0.8443 for $J/W = 0.1$ and 3 , respectively.

compressibility and the multifractal dimensions take the form [17]

$$\chi \approx 1/g \quad \text{and} \quad D_q \approx 1 - q/g. \quad (25)$$

As for the RSE, here Eqs. (25) satisfy relation (3). Again, by direct substitution of Eqs. (25) we verified that Eqs. (12-15) are satisfied at leading order in $1/g$, $g \gg 1$.

We want to mention that in [17] it was shown that Eq. (25) reproduces well the numerically obtained D_1 but underestimates the numerical D_2 , in particular for small g , see Fig. 7. Now, notice that by plotting the numerically obtained $D_1/(2 - D_1)$ we nicely reproduce the numerical data for D_2 , that is Eq. (15) works well also for this model. Then, if we take $D_1 \approx 1 - 1/g$ as the theoretical prediction for D_1 and plug it into Eq. (15) we get

$$D_2 \approx (1 - 1/g)(1 + 1/g)^{-1}, \quad (26)$$

which in fact works much better than $D_2 \approx 1 - 2/g$ in reproducing the numerical D_2 , see Fig. 7.

To get the expression for D_q we substituted $\chi \approx 1/g$ or $D_1 \approx 1 - 1/g$ into Eq. (12) or (13), respectively, to get

$$D_q \approx (g-1)(g+q-1)^{-1}. \quad (27)$$

In Fig. 8 we plot D_q as a function of q for the IQM model for some values of g . We also plot Eq. (27) and observe that it falls below the numerical data mainly for small g . However, by substituting the numerically obtained values of D_1 into Eq. (13) we get much better correspondence with the numerical D_q , mainly for $1 < q < 2$. In Fig. 8 we also include D_q from Eq. (25). We may conclude that while Eq. (25) reproduces well the numerical D_q for $q < 1$, Eq. (27) can serve as the analytical continuation for $q > 1$.

The critical ultrametric ensemble. The critical ultrametric ensemble (CUE) proposed in [18] consists of $2^K \times 2^K$ Hermitian matrices whose matrix elements are Gaussian random variables with zero mean and variance

$$\langle |H_{mm}|^2 \rangle = W^2, \quad \langle |H_{mn}|^2 \rangle = 2^{2-d_{mn}} J^2, \quad (28)$$

where d_{mn} is the ultrametric distance between m and n on the binary tree with K levels and the root of 1. The parameter in this model is the ratio J/W . For the CUE, when $J/W \ll 1$, the compressibility and the multifractal dimensions have the form [4, 18]

$$\chi = 1 - \frac{J}{W} \frac{\pi}{\sqrt{2} \ln 2} \quad \text{and} \quad D_q = \frac{J}{W} \frac{\sqrt{\pi} \Gamma(q-1/2)}{\sqrt{2} \ln 2 \Gamma(q)}. \quad (29)$$

Eqs. (29) satisfy relation (3) at first order in J/W [4]. Again, as for the previous critical ensembles, by direct substitution of Eqs. (29) we verified that Eqs. (12-15) are satisfied at leading order in J/W , for $0.8 < q < 2.5$; because in this range of q we have that $\Gamma(q-0.5)/\sqrt{\pi}\Gamma(q) \approx 1/q$.

In Fig. 9 we show D_q as a function of q for the CUE for $J/W = 0.1$ and 3. The data was taken from [18]. The blue dashed line is D_q from Eq. (29) for $J/W = 0.1$. Notice that since Eq. (29) is only valid when $J/W \ll 1$ and for $q \geq 3/4$ one can not use it to predict D_q for $J/W = 3$. However, with Eq. (13) using as input the numerically obtained D_1 we got good predictions for D_q for small and large values of J/W and even for values of q smaller than $3/4$. This is shown in Fig. 9 where we plot Eq. (13) (red dashed lines) using $D_1 = 0.2805$ and 0.8443 for $J/W = 0.1$ and 3, respectively. The values of D_1 were obtained by the interpolation of the D_q data. We observe good correspondence between Eq. (13) and the numerical D_q for $0 < q < 10$.

Conclusions. — In this paper we propose heuristic relations on one hand between the generalized multifractal dimensions, D_q and $D_{q'}$, for a relatively wide range of the parameters q and q' , and on the other hand between these dimensions and the level compressibility χ . As a result we find a general framework embracing an earlier [7] and a recent one [4]. Our proposed relations have been backed by numerical simulation on various random matrix ensembles whose eigenstates have multifractal properties. These

results call for further theoretical as well as numerical investigations.

The authors are greatly indebted to V. Kravtsov for useful discussions. This work was partially supported by VIEP-BUAP (Grant No. MEBJ-EXC10-I), the Alexander von Humboldt Foundation, and the Hungarian Research Fund (OTKA) grants K73361 and K75529.

REFERENCES

- [1] JANSSEN M., *Phys. Rep.*, **295** (1998) 1; *Int. J. Mod. Phys. B*, **8** (1994) 943.
- [2] EVERS F. and MIRLIN A. D., *Rev. Mod. Phys.*, **80** (2008) 1355.
- [3] RICHARDELLA A., ROUSHAN P., MACK S., ZHOU B., HUSE D. A., AWSCHALOM D. D. and YAZDANI A., *Science*, **327** (2010) 665; FAEZ S., STRYBULEVYCH A., PAGE J. H., LAGENDIJK A. and VAN TIGGELEN B. A., *Phys. Rev. Lett.*, **103** (2009) 155703; HASHIMOTO K., SOHRMANN C., WIEBE J., INAKA T., MEIER F., HIRAYAMA Y., RÖMER R. A., WIESENDANGER R. and MORGENSTERN M., *Phys. Rev. Lett.*, **101** (2008) 256802.
- [4] BOGOMOLNY E. and GIRAUD O., *Phys. Rev. Lett.*, **106** (2011) 044101.
- [5] BOGOMOLNY E. and GIRAUD O., *Phys. Rev. E*, **184** (2011) 036212; arXiv:1112.2164.
- [6] RUSHKIN I., OSSIPOV A. and FYODOROV Y., *J. Stat. Mech.*, (2011) L03001
- [7] CHALKER J. T., KRAVTSOV V. E. and LERNER I. V., *JETP Lett.*, **64** (1996) 386; KLESSE R. and METZLER M., *Phys. Rev. Lett.*, **79** (1997) 721;
- [8] MÉNDEZ-BERMÚDEZ J. A., ALCÁZAR-LÓPEZ A. and VARGA I., unpublished.
- [9] MIRLIN A. D., FYODOROV Y. V., DITTES F.-M., QUEZADA J. and SELIGMAN T. H., *Phys. Rev. E*, **54** (1996) 3221.
- [10] MIRLIN A. D., *Phys. Rep.*, **326** (2000) 259.
- [11] KRAVTSOV V. E. and MUTTALIB K. A., *Phys. Rev. Lett.*, **79** (1997) 1913; KRAVTSOV V. E. and TSVELIK A. M., *Phys. Rev. B*, **62** (2000) 9888.
- [12] CUEVAS E., ORTUNO M., GASPARIAN V. and PEREZ-GARRIDO A., *Phys. Rev. Lett.*, **88** (2001) 016401.
- [13] VARGA I. and BRAUN D., *Phys. Rev. B*, **61** (2000) R11859; VARGA I., *Phys. Rev. B*, **66** (2002) 094201.
- [14] MÉNDEZ-BERMÚDEZ J. A., KOTTOS T. and COHEN D., *Phys. Rev. E*, **73** (2006) 036204; MÉNDEZ-BERMÚDEZ J. A. and VARGA I., *Phys. Rev. B*, **74** (2006) 125114.
- [15] KRAVTSOV V. E., OSSIPOV A., YEVTUSHENKO O. M. and CUEVAS E., *Phys. Rev. B*, **82** (2010) 161102(R).
- [16] BOGOMOLNY E., GIRAUD O. and SCHMIT C., *Phys. Rev. Lett.*, **103** (2009) 054103.
- [17] MARTIN J., GIRAUD O. and GEORGEOT B., *Phys. Rev. E*, **77** (2008) 035201(R).
- [18] FYODOROV Y. V., OSSIPOV A. and RODRIGUEZ A., *J. Stat. Mech.*, (2009) L12001.